Atom-based power-frequency electric field measurement using the radio-frequency-modulated Rydberg spectroscopy

Weixin Liu(刘伟新)[1,2], Linjie Zhang(张临杰)[3,2,†], and Tao Wang(汪涛)[4,5,‡]

[1] *Institute of Theoretical Physics and Department of Physics, State Key Laboratory of Quantum Optics and Quantum Optics Devices, Shanxi University, Taiyuan* 030006, *China*

[2] *Collaborative Innovation Center of Extreme Optics, Taiyuan* 030006, *China*

[3] *State Key Laboratory of Quantum Optics and Quantum Optics Devices, Institute of Laser Spectroscopy, Shanxi University, Taiyuan* 030006, *China*

[4] *Department of Physics, and Center of Quantum Materials and Devices, Chongqing University, Chongqing* 401331, *China*

[5] *Center of Modern Physics, Institute for Smart City of Chongqing University in Liyang, Liyang* 213300, *China*

(Received 5 November 2022; revised manuscript received 15 November 2022; accepted manuscript online 29 November 2022)

The radio-frequency modulated electromagnetically induced transparency (EIT) in a ladder three-level system with Rydberg state is studied. Under the influence of a fast radio-frequency field, the EIT peak splits into a series of sidebands. When attaching a power-frequency electric field directly to the fast radio-frequency field, the odd-order sidebands of the Rydberg-EIT oscillate sensitively with the power-frequency field. The oscillation frequency is equal to twice the power frequency; the oscillation amplitude is monotonically increasing with the amplitude of the power-frequency field when the change of Stark-shift is smaller than the radio frequency. Our work paves the way for measurement of power-frequency electric field based on Rydberg atoms.

Keywords: Rydberg atom, electromagnetically induced transparency spectrum, power-frequency electric field

PACS: 32.80.Ee, 42.50.Gy, 84.40.–x **DOI:** 10.1088/1674-1056/aca6db

1. Introduction

Precise measurement of power-frequency (50 Hz or 60 Hz) electric field around high-voltage equipment is important not only to design and running status monitor of electric equipment but also to human health and safety.[1–3] However, traditional methods based on electromagnetic induction or optical effect have obvious shortcomings in precisely measuring power-frequency (pf) electric field. For example, they are difficult to apply to the on-site field measurement, as well as to measure the strong electric field. Noticeably, the measurement based on electromagnetic induction using electric field sensors may cause a distortion on original electric field, and on optical effect using optical fiber is subject to the temperature fluctuation.[4–6]

Recently, Rydberg atom-based microwave electrometry has attracted extensive attention due to its extraordinary reproducibility, accuracy and stability.[7–20] Thus, the approach of utilizing the electromagnetically induced transparency (EIT) and Autler–Townes (AT) splitting has the potential for a new international standard for electric-field measurements and calibrations. On the other hand, when a radio-frequency (rf) field is applied to the system, the Rydberg levels experience ac Stark shifts. When the rf field increases, the energy level of the Rydberg state is split into a series of quasi-stationary Floquet bands, which generate the EIT sidebands. In the presence of a pure harmonic ac field, only the even-order sidebands appear (i.e., sidebands separated by even multiples of the rf driving frequency); when an additional dc field offset is applied, the odd-order sidebands begin to emerge (i.e., sidebands separated by odd multiples of the rf driving frequency). The rf-modulated Rydberg-EIT has been investigated and observed in many experiments, and be applied to rf field calibration and polarization measurement,[21–25] but has not yet been used to the pf field measurement.

In this work, we propose a method to measure the pf electric field based on the rf-modulated Rydberg atom with EIT. We present a detailed theoretical description and analysis of the ac-Stark effect of the Rydberg state under both the pf- and rf-modulation in a three-level ladder system. We first derive the effective Hamiltonian of the driven system, and then get the theoretical expression for the driven EIT by solving the equation of the motion for density matrix and getting the steady-state solution. Based on the effective Hamiltonian, we theoretically show that the driven Rydberg-EIT spectra only exhibit even-order sidebands when applying a pure ac electric field, and the odd-order sidebands appear in the presence of the pf electric field, which acts as a slow-varying dc-like field offset. In addition, odd-order sidebands will oscillate sensitively with the pf field. With the help of the oscillation intensity and frequency of the odd-sidebands, we can measure the amplitude and frequency of the pf electric field. The sensitivity of sidebands with respect to the pf field is analyzed, and the up-

†Corresponding author. E-mail: zlj@sxu.edu.cn

‡Corresponding author. E-mail: tauwaang@cqu.edu.cn

© 2023 Chinese Physical Society and IOP Publishing Ltd

per bound of the amplitude of the pf field that can be measured is given to be related to the polarizability of the Rydberg state and driving frequency of the rf electric field. Finally, we also give the specific measurement scheme and steps.

2. The model

2.1. Effective Hamiltonian of the system

We consider a three-level, ladder configuration system as shown in Fig. 1, in which a weak probe laser is coupled to the transition between the ground state $|1\rangle$ and excited state $|2\rangle$, and the coupling laser is scanned through resonance with the transition between the excited state and a Rydberg state $|3\rangle$. In addition, an additional electric field $\varepsilon(t)$ is applied to the system, and its frequency with the order of tens of MHz is much less than the relevant optical transition frequency, i.e., the frequency difference of the excited state and the Rydberg state. The Rydberg state is extremely sensitive to the electric field, the energy of the Rydberg state will be shifted in the applied electric field due to the ac Stark effect. Because this applied electric field is weak enough, the energy shift of the Rydberg state can be calculated with perturbation theory. The second-order perturbation gives the instantaneous frequency of the Rydberg state $\omega_3(t) = \omega_3 - \alpha\varepsilon^2(t)/2\hbar$, where ω_3 is the unperturbed bare frequency of the Rydberg state in the absence of rf electric field, α is the dipole polarizability of the Rydberg state.

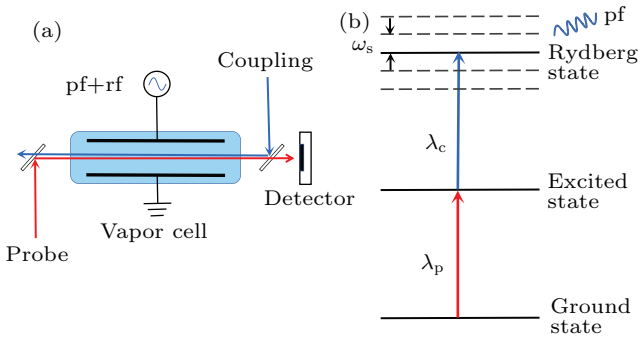


Fig. 1. (a) Schematic of the vapor cell setup for measuring EIT with the probe and coupling beams counter-propagating through the vapor cell. The additional (pf + rf) electric field is applied to the two electrode plates. The transmission of the probe beam through the cell is monitored by the detector. (b) Energy-level scheme of the driven Rydberg-EIT. The probe laser (λ_p) is resonant with the ground-excited state transition, and the coupling laser (λ_c) is canned through the excited-Rydberg state transition. The Rydberg state splits into a series of Floquet band with the intervals ω_s under the modulation of both power-frequency (ω_0) and radio-frequency (ω_s) electric field. At the same time, each band experiences a slow oscillation with the power-frequency field.

Then the Hamiltonian of the system can be expressed as

$$\hat{H} = \hat{H}_0 + \hat{H}_1, \tag{1}$$

where

$$\hat{H}_0 = \hbar\omega_1|1\rangle\langle 1| + \hbar\omega_2|2\rangle\langle 2| + \hbar[\omega_3 + f(t)]|3\rangle\langle 3| \tag{2}$$

with $f(t) = -\alpha\varepsilon^2(t)/2\hbar$, and the atom-field Hamiltonian $\hat{H}_1$ in the electric-dipole approximation can be expressed as

$$\begin{aligned}\hat{H}_1 = &-\frac{\hbar}{2}\left[\Omega_p(e^{-i\omega_p t} + e^{i\omega_p t})|1\rangle\langle 2| + \text{H.c.}\right] \\ &-\frac{\hbar}{2}\left[\Omega_c(e^{-i\omega_c t} + e^{i\omega_c t})|2\rangle\langle 3| + \text{H.c.}\right],\end{aligned} \tag{3}$$

where ω_p and ω_c are the angular frequencies of the probe and coupling laser. Ω_p and Ω_c are the Rabi frequencies corresponding to the transitions $|1\rangle \leftrightarrow |2\rangle$ and $|2\rangle \leftrightarrow |3\rangle$, respectively. We turn the system to the interaction picture by the unitary operator $\hat{U}_1 = e^{-\frac{i}{\hbar}\int_0^t \hat{H}_0(\tau)\,d\tau}$, which gives the interaction picture Hamiltonian

$$\begin{aligned}\hat{H}_I = &-\frac{\hbar}{2}\left[\Omega_p(e^{-i\omega_p t} + e^{i\omega_p t})e^{-i\omega_{21}t}|1\rangle\langle 2| + \text{H.c.}\right] \\ &-\frac{\hbar}{2}\left[\Omega_c(e^{-i\omega_c t} + e^{i\omega_c t})e^{-i\int_0^t[\omega_{32}+f(\tau)]\,d\tau}|2\rangle\langle 3|\right. \\ &\left.+\text{H.c.}\right],\end{aligned} \tag{4}$$

where $\omega_{21} = \omega_2 - \omega_1$ and $\omega_{32} = \omega_3 - \omega_2$.

Now we take the applied electric field as consisting of a pf field and an ac field

$$\varepsilon(t) = \varepsilon_{pf} + \varepsilon_{ac}\cos(\omega_s t), \tag{5}$$

where $\varepsilon_{pf} = \varepsilon_0\cos(\omega_0 t)$ is the pf field with ε_0 and ω_0 being the amplitude and frequency of the pf field, respectively. Due to the frequency of the pf field much smaller than the rf ac frequency ω_s with the order of MHz as well as the other system energy scales, we can treat the pf field as a slowly varying dc-like part under the fast ac field modulation. Thus, in the time scale $1/\omega_s$ we handle in the following, the pf field ε_{pf} can be treated as being time-static. Then

$$e^{-i\int_0^t f(\tau)\,d\tau} = e^{\frac{i\alpha}{4\hbar}(2\varepsilon_{pf}^2 + \varepsilon_{ac}^2)t}A(t), \tag{6}$$

where

$$A(t) = e^{\frac{i\alpha}{8\hbar\omega_s}(\varepsilon_{ac}^2\sin 2\omega_s t + 8\varepsilon_{pf}\varepsilon_{ac}\sin\omega_s t)} \tag{7}$$

is the time-periodic term that can be expanded in a Fourier series as $A(t) = \sum_{l=-\infty}^{+\infty} A_l e^{il\omega_s t}$ with the Fourier coefficients

$$A_l = \sum_{k=-\infty}^{+\infty} J_k\left(\frac{\alpha\varepsilon_{ac}^2}{8\hbar\omega_s}\right) J_{l-2k}\left(\frac{\alpha\varepsilon_{pf}\varepsilon_{ac}}{\hbar\omega_s}\right), \tag{8}$$

where $J_k(z)$ is the Bessel function of the first kind. Then the interaction picture Hamiltonian (4) can be rewritten as

$$\begin{aligned}\hat{H}_I = &-\frac{\hbar}{2}\left[\Omega_p(e^{-i\omega_p t} + e^{i\omega_p t})e^{-i\omega_{21}t}|1\rangle\langle 2| + \text{H.c.}\right] \\ &-\frac{\hbar}{2}\left[\sum_l \Omega_c A_l(e^{-i\omega_c t} + e^{i\omega_c t})e^{-i(\omega_{32}-\omega_\alpha - l\omega_s)t}|2\rangle\langle 3|\right. \\ &\left.+\text{H.c.}\right],\end{aligned} \tag{9}$$

where $\omega_\alpha = \alpha\varepsilon_{pf}^2/2\hbar + \alpha\varepsilon_{ac}^2/4\hbar$ is the Stark shift due to the dc field and the rf amplitude.[21]

The analytical calculation of the spectrum with the Hamiltonian (9) is difficult in the general case. However, we could make the rotating-wave approximation (RWA) if these conditions are satisfied, (i) the coupling of probe laser is much weaker than the corresponding transition, i.e., $\Omega_{\rm p} \ll \omega_{21}$; (ii) the Rabi frequency $\Omega_{\rm c}$ is weak enough compared to the frequency of the rf field, i.e., $\Omega_{\rm c} \ll \omega_{\rm s}$ (please note that $\omega_{\rm s}$ is much less than ω_{32}). The second condition (ii) implies that the intervals ($\omega_{\rm s}$) between adjacent sidebands are much larger than their linewidths (proportional to $\Omega_{\rm c}$), thus all the sidebands can be treated as resolvable.[22,26] With these conditions, when the probe laser is near resonance, and the coupling laser is close to one sideband resonance, i.e., $\omega_{\rm p} \approx \omega_{21}$ and $\omega_{\rm c} \approx \omega_{32} - \omega_\alpha - n\omega_{\rm s}$, we can neglect the other non-resonant terms that oscillate rapidly, then the interaction picture Hamiltonian (9) just for n-th sideband can be simplified to

$$\hat{H}^{\rm n}_{\rm RWA} = -\frac{\hbar}{2}\left(\Omega_{\rm p}\,{\rm e}^{{\rm i}\Delta_{\rm p}t}|1\rangle\langle 2| + \Omega_{\rm c}^{n}\,{\rm e}^{{\rm i}\Delta_{\rm c}^{n}t}|2\rangle\langle 3|\right) + {\rm H.c.}, \quad (10)$$

where

$$\Delta_{\rm c}^{n} = \Delta_{\rm c} + \omega_\alpha + n\omega_{\rm s},\ \ \Delta_{\rm c} = \omega_{\rm c} - \omega_{32},\ \ \Delta_{\rm p} = \omega_{\rm p} - \omega_{21}, \quad (11)$$

and $\Omega_{\rm c}^{n}$ is the effective Rabi frequency of the coupling laser for n-th sideband,

$$\Omega_{\rm c}^{n} = \Omega_{\rm c} A_n,\ \ A_n = \sum_{k=-\infty}^{+\infty} J_k\left(\frac{\alpha\varepsilon_{\rm ac}^2}{8\hbar\omega_{\rm s}}\right) J_{n-2k}\left(\frac{\alpha\varepsilon_{\rm pf}\varepsilon_{\rm ac}}{\hbar\omega_{\rm s}}\right). \quad (12)$$

Now we transform the Hamiltonian (10) back with the unitary operator $\hat{U}_2 = |1\rangle\langle 1| + {\rm e}^{-{\rm i}\Delta_{\rm p}t}|2\rangle\langle 2| + {\rm e}^{-{\rm i}(\Delta_{\rm p}+\Delta_{\rm c}^{n})t}|3\rangle\langle 3|$ and get the effective Hamiltonian for n-th sideband as

$$\hat{H}^{n}_{\rm eff} = -\frac{\hbar}{2}\begin{pmatrix} 0 & \Omega_{\rm p} & 0 \\ \Omega_{\rm p}^{*} & 2\Delta_{\rm p} & \Omega_{\rm c}^{n} \\ 0 & \Omega_{\rm c}^{n*} & 2(\Delta_{\rm p}+\Delta_{\rm c}^{n}) \end{pmatrix}. \quad (13)$$

2.2. The driven electromagnetically induced transparency

From a density matrix analysis, for the n-th sideband, the system can be described by the master equation[27]

$$\dot{\rho} = -\frac{\rm i}{\hbar}[\hat{H}^{n}_{\rm eff}, \rho] - \frac{1}{2}\{\Gamma, \rho\}, \quad (14)$$

where Γ is the relaxation matrix defined by $\langle i|\Gamma|j\rangle = \gamma_i\delta_{ij}$ with γ_i being the natural decay rate of level $|i\rangle$. Then we can get the steady-state solution for ρ_{21} in the weak probe limit[28]

$$\rho_{21} = \frac{{\rm i}\Omega_{\rm p}^{*}/2}{\gamma_{21} - {\rm i}\Delta_{\rm p} + \frac{|\Omega_{\rm c}^{n}|^2/4}{\gamma_{31} - {\rm i}(\Delta_{\rm p}+\Delta_{\rm c}^{n})}}. \quad (15)$$

In general, the atoms in the medium have a nonzero velocity distribution due to the temperature in typical experiments. Considering that the probe beam and coupling laser are counterpropagating, the atom moving towards the probe laser with velocity v feels its frequency approximately upshifted by $\omega_{\rm p}v/c$, meanwhile the frequency of the coupling laser that the atom feels downshifted approximately by $\omega_{\rm c}v/c$. Then we can get the Doppler averaged susceptibility χ, the imaginary part of which indicates the absorption characteristic of the medium, by integrating over velocity

$$\chi = \int \frac{{\rm i}N(v)|\mu_{12}|^2/\hbar\varepsilon_0}{\gamma_{21} - {\rm i}\Delta_{\rm p} - {\rm i}\omega_{\rm p}\frac{v}{c} + \frac{|\Omega_{\rm c}^{n}|^2/4}{\gamma_{31} - {\rm i}(\Delta_{\rm p}+\Delta_{\rm c}^{n}) - {\rm i}(\omega_{\rm p}-\omega_{\rm c})\frac{v}{c}}}\,{\rm d}v, \quad (16)$$

where $N(v) = N_0\exp(-v^2/u^2)/(u\sqrt{\pi})$, μ_{12} is the dipole matrix element corresponding to the transition $|1\rangle \leftrightarrow |2\rangle$, N_0 is the total density of atoms in the cell, $u = \sqrt{2k_{\rm B}T/m}$ is the most probable velocity with $k_{\rm B}$ the Boltzmann constant, m is the mass of the atom, and T is medium temperature. Finally we can get the total susceptibility by summing the contribution from all the sidebands, $\chi^{\rm Tot} = \sum_n \chi$, and then get the whole driven EIT spectra.

3. Results

Now we present a specific example for the measurement of the pf electric field based on the driven Rydberg-EIT. Considering a ^{133}Cs three-level system: $6S_{1/2}$–$6P_{3/2}$–$53S_{1/2}$ in a vapor cell at a controlled temperature of 300 K. The Rydberg state $53S_{1/2}$ is driven by an rf field with an ac frequency $\omega_{\rm s}/2\pi = 30$ MHz, which is much larger than the Rydberg relaxation rate γ_3 with the order of tens of kHz. The polarizability of the Rydberg state $53S_{1/2}$ is $\alpha = \hbar \times 71.1$ MHz/[V/cm]^2.[29] We also set $\Gamma_1 = 0$ and $\Gamma_2/2\pi = 5$ MHz, the coupling Rabi frequency $\Omega_{\rm c}/2\pi = 5$ MHz. The wavelengths of probe and coupling laser are chosen at $\lambda_{\rm p} = 852$ nm and $\lambda_{\rm c} = 510$ nm to induce the corresponding transitions, respectively.

From the above analysis, we can see that when only the ac field applied, i.e., $\varepsilon_{\rm pf} = 0$, there is no odd-order sidebands in the EIT spectra due to the effective coupling Rabi frequency [Eq. (12)] is zero when n is odd. When both the dc-like pf field and ac field applied, the EIT spectra presents a series of sidebands separated by interval $\omega_{\rm s}$.[21,22] Each EIT sideband is governed by the effective Hamiltonian (13). Thus, the pf field accounts for the emergence of the odd-order sidebands. This is the key point of the idea to measure the pf electric field.

In Fig. 2 we show the driven Rydberg-EIT under the effect of the rf field for different combinations of pf and ac electric fields at a fixed time. We can see that when a pure ac field applied as shown in Fig. 2(b), the Rydberg-EIT spectra only show the even-order sidebands, which are marked by $n = \pm 2$ in the blue circles, and the spacing between the adjacent sidebands is $2\omega_{\rm s}$. Meanwhile, the main peak is shifted by the Stark shift ω_α, compared to Fig. 2(a) in the absence of any applied electric field. When further applying the pf filed, as shown in Figs. 2(c) and 2(d), the odd-order sidebands appear, marked by $n = \pm 1$. The odd-order sidebands are enhanced with increasing the amplitude of pf field as can be seen by comparing

Figs. 2(c) and 2(d). In addition, the other higher sidebands are invisible because the effective coupling Rabi frequencies [Eq. (12)] are too small for $n > 2$.

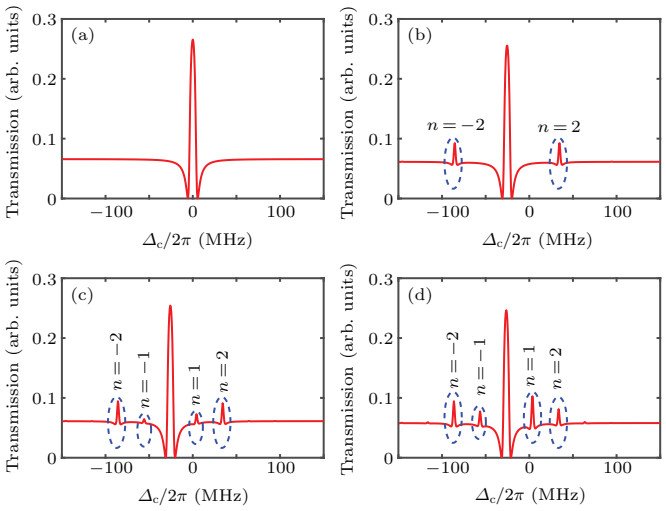


Fig. 2. The driven Rydberg-EIT spectra with an applied electric field. (a) EIT spectra without any applied field. (b) EIT spectra under a pure ac field, i.e., $\varepsilon_{pf} = 0$, $\varepsilon_{ac} = 3$ V/cm, and $\omega_s/2\pi = 30$ MHz. (c) and (d) The EIT spectra under both pf and ac fields at $t = 0$ with $\varepsilon_{ac} = 3$ V/cm, $\omega_s/2\pi = 30$ MHz; $\varepsilon_0 = 0.2$ V/cm in (c) and $\varepsilon_0 = 0.4$ V/cm in (d). The peaks in the blue circles indicate the corresponding sidebands.

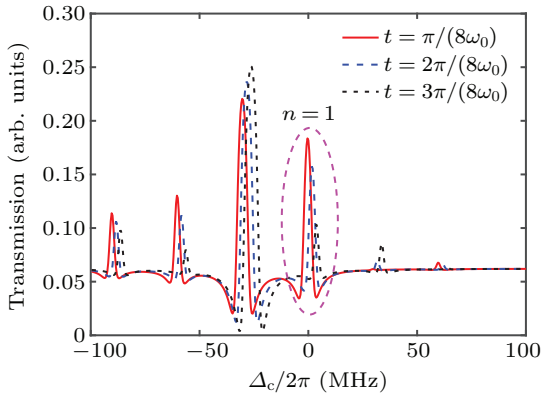


Fig. 3. The driven Rydberg-EIT spectra for an applied ac electric field with $\varepsilon_{ac} = 3$ V/cm, $\omega_s/2\pi = 30$ MHz and a power-frequency electric field with $\varepsilon_0 = 1$ V/cm, $\omega_0/2\pi = 50$ Hz at different times: $t = \pi/(8\omega_0)$ for the solid red line, $t = \pi/(4\omega_0)$ for the dashed blue line, and $t = 3\pi/(8\omega_0)$ for the dotted black line. The peak in the magenta circle indicates the +1-order sideband.

On the other hand, the locations and magnitudes of all the EIT sidebands will oscillate with the pf field due to the time-period Stark shift ω_α in Eq. (11) and effective coupling Rabi frequency [Eq. (12)]. However, due to the odd-order sidebands appearing on account of pf field, we realize that the odd-order sidebands are more sensitive to the pf field. In Fig. 3 we show the driven EIT spectra at different times. It is shown that the first-order sideband ($n = 1$) indeed changes most dramatically with the pf field. In order to further verify this, we compare the sensitivity of all the five visible sidebands to the pf field. We lock the coupling detuning at the first-order sideband, i.e., $\Delta_c = -\omega_\alpha + \omega_s$ at $t = 0$ and measure the intensity of the EIT sidebands over time. As shown in Fig. 4, the oscillation amplitudes of the first-order sideband is greater than others. Hence, we can focus on the +1-order sideband to implement the measurement.

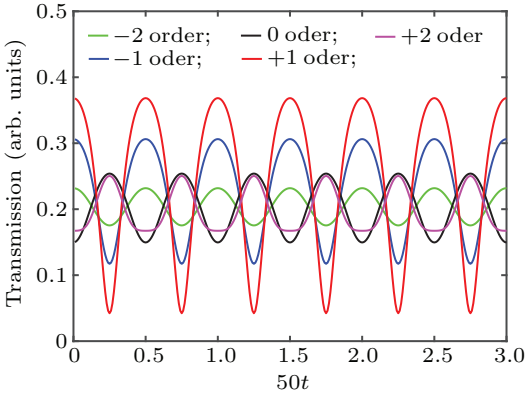


Fig. 4. Oscillation of different sidebands of the Rydberg-EIT with $\varepsilon_{ac} = 3$ V/cm, $\omega_s/2\pi = 30$ MHz, $\varepsilon_0 = 1$ V/cm, and $\omega_0/2\pi = 50$ Hz.

To further measure the amplitude and frequency of the pf electric field, in Fig. 5 we show the oscillation of the +1-order sideband under different amplitudes of the pf field with the frequencies (a) $\omega_0/2\pi = 50$ Hz and (b) $\omega_0/2\pi = 60$ Hz. It is shown that the +1-order sideband oscillates with a frequency equal to twice the frequency of the pf field. In addition, the oscillation intensity increases with increasing the amplitude of the pf field.

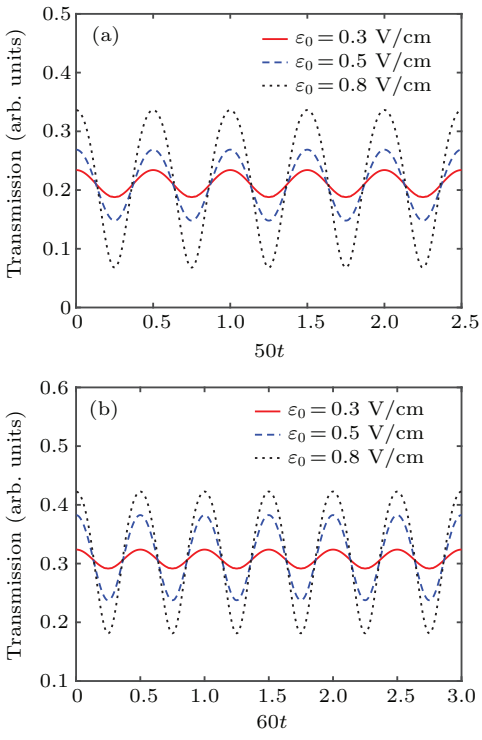


Fig. 5. Oscillation of the +1-order sideband of the Rydberg-EIT under different power-frequency amplitudes ε_0 with (a) $\omega_0/2\pi = 50$ Hz and (b) $\omega_0/2\pi = 60$ Hz.

We also investigate the contrast of the oscillation curve of the +1-order sideband with respect to the amplitude of the pf field ε_0. Here the contrast (ΔT) is defined as the difference between the maximum and the minimum amplitudes of the oscillation. In Fig. 6 we show the contrast changing with ε_0

under different rf frequencies for Fig. 6(a) $\omega_s/2\pi = 30$ MHz and Fig. 6(b) $\omega_s/2\pi = 50$ MHz. We can see that the contrast is monotonically increasing with ε_0 until $\varepsilon_0 \simeq 2$ V/cm in Fig. 6(a) and $\varepsilon_0 \simeq 3$ V/cm in Fig. 6(b). Here we give a explanation to the emergence of the non-monotonicity. Due to the existence of the pf field, the Stark shift ω_α also changes with time. When the change of ω_α is closed to the sideband interval ω_s, the adjacent sidebands will interfere each other when measuring the EIT signal at a fix detuning. Then the non-monotonicity of the contrast emerges. This also gives a upper bound of the pf field amplitude that can be measured with the EIT oscillation curves as shown in Fig. 5. Namely, the maximum change of the Stark shift ω_α should be smaller than the frequency of the ac field–the sidebands interval, which gives $\varepsilon_0 < \sqrt{2\hbar\omega_s/\alpha}$.

On the other hand, we can see from Fig. 3 that all the sidebands are oscillating with the pf field. Considering the measurement time of scanning the coupling laser in an actual experiment, there may be some distortion in the driven-EIT spectrum. In addition, it seems hard to fix the detuning at the first-order sideband to measure the oscillation as shown in Fig. 5. However, all the sidebands oscillate with the pf field, and only appear in some special detuning separated by integer ω_s. We can first fix the detuning at any peak appearing position (even with a distortion), and can get a rough oscillation frequency as shown in Figs. 4 and 5. Second, we can scan the detuning just with integer oscillation periods. Likewise, we can get the driven-EIT spectrum with the same pf field, and then fix the detuning at the sidebands. After that, we can implement the pf field measurement. Obviously, we can repeat such a process to improve the accuracy.

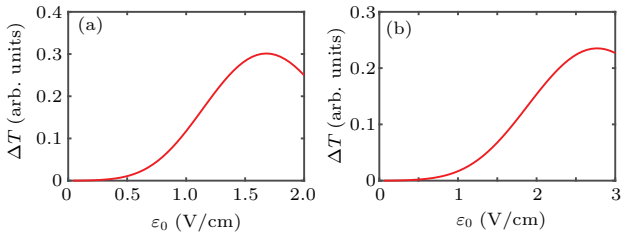


Fig. 6. The contrast (ΔT) of the oscillation of the +1-order sideband a function of ε_0 with (a) $\omega_s/2\pi = 30$ MHz and (b) $\omega_s/2\pi = 50$ MHz.

4. Conclusion

In conclusion, we have theoretically studied the driven Rydberg-EIT under the effect of the rf electric field in a ladder three-level system. When applying a slow pf electric field and a fast ac field, the odd-order sidebands are sensitive to the pf field. Based on the odd-order sidebands, we can implement a measurement of the pf electric field. The amplitude and frequency of the pf field can be inferred from the oscillation intensity and frequency of the odd-order sidebands, respectively. We also give the upper bound of the amplitude of the pf field that can be measured. Our work paves the way for self-calibration measurement of the power-frequency electric field based on the Rydberg-atom EIT.

Acknowledgements

This work was supported by the National Natural Science Foundation of China (Grant No. 12274045), the Special Foundation for Theoretical Physics Research Program of China (Grant No. 11647165), and the China Postdoctoral Science Foundation Funded Project (Grant No. 2020M673118).

References

[1] Zhu W Q, Guo J, Zhang G Z, Yao D G, Zhang S Y and Qian S L 2019 *Procedia Comput. Sci.* **155 740–745**
[2] Xiao D P, Ma Q C, Xie Y T, Zheng Q and Zheng Z L 2018 *Sensors* **18** 1053
[3] Zhang X, Bai Q, Xia S H, Zheng F J and Chen S F 2006 *Chin. J. Sci. Instrum.* **27** 1433 (in Chinese)
[4] Chen F S and Bin S 2010 *Semiconduct. Optoelectron.* **31** 202
[5] Jiang Y Z, Yang D W and Zhang F J 2014 *Laser Optoelectron. Prog.* **51** 022301
[6] Li Z Y, Yuan H W, Cui Y, Ding Z and Zhao L X 2019 *IEEE Trans. Instrum. Meas.* **68** 1132
[7] Mohapatra A K, Jackson T R and Adams C S 2007 *Phys. Rev. Lett.* **98** 113003
[8] Degen C L, Reinhard F and Cappellaro P 2017 *Rev. Mod. Phys.* **89** 035002
[9] Sedlacek J A, Schwettmann A, Kübler H and Shaffer J P 2013 *Phys. Rev. Lett.* **111** 063001
[10] Sedlacek J A, Schwettmann A, Kübler H, Löw R, Pfau T and Shaffer J P 2012 *Nat. Phys.* **8** 819
[11] Zhang L, Liu J, Jia Y, Zhang H, Song Z and Jia S 2018 *Chin. Phys. B* **27** 033201
[12] Hao L, Xue Y, Fan J, Jiao Y, Zhao J and Jia S 2019 *Chin. Phys. B* **28** 053202
[13] Jing M, Hu Y, Ma J, Zhang H, Zhang L, Xiao L and Jia S 2020 *Nat. Phys.* **16** 911
[14] Hao L, Xue Y, Fan J, Bai J, Jiao Y and Zhao J 2020 *Chin. Phys. B* **29** 033201
[15] Liu X, Jia F, Zhang H, Mei J, Yu Y, Liang W, Zhang J, Xie F and Zhong Z 2021 *AIP Adv.* **11** 085127
[16] Zhang L H, Liu Z K, Liu B, Zhang Z Y, Guo G C, Ding D S and Shi B S 2022 *Phys. Rev. Appl.* **18** 014033
[17] Liu Z K, Zhang L H, Liu B, Zhang Z Y, Guo G C, Ding D S and Shi B S 2022 *Nat. Commun.* **13** 1997
[18] Liu B, Zhang L H, Liu Z K, Zhang Z Y, Zhu Z H, Gao W, Guo G C, Ding D S and Shi B S 2022 *Phys. Rev. Appl.* **18** 014045
[19] Ding D S, Liu Z K, Shi B S, Guo G C, Mølmer K and Adams C S 2022 *Nat. Phys.* **18** 1447
[20] Liu X B, Jia F D, Zhang H Y, Mei J, Liang W C, Zhou F, Yu Y H, Liu Y, Zhang J, Xie F and Zhong Z P 2022 *Chin. Phys. B* **31** 090703
[21] Zhang Y, Ciocca M, He L W, Burkhardt C E and Leventhal J J 1994 *Phys. Rev. A* **50** 1101
[22] Bason M G, Tanasittikosol M, Sargsyan A, Mohapatra A K, Sarkisyan D, Potvliege R M and Adams C S 2010 *New J. Phys.* **12** 065015
[23] Miller S A, Anderson D A and Raithel G 2016 *New J. Phys.* **18** 053017
[24] Jiao Y, Hao L, Han X, Bai S, Raithel G, Zhao J and Jia S 2017 *Phys. Rev. Appl.* **8** 014028
[25] Anderson D A, Miller S A, Raithel G, Gordon J A, Butler M L and Holloway C L 2016 *Phys. Rev. Appl.* **5** 034003
[26] Silveri M P, Tuorila J A, Thuneberg E V and Paraoanu G S 2017 *Rep. Prog. Phys.* **80** 056002
[27] Scully M O and Zubairy M S 1997 *Quantum Optics* (Cambridge: Cambridge University Press)
[28] Gea-Banacloche J, Li Y Q, Jin S Z and Xiao M 1995 *Phys. Rev. A* **51** 576
[29] He X H, Li B W and Zhang C X 1989 *Acta Phys. Sin.* **38** 1717 (in Chinese)